

# Synthesis, Characterization and Mechanical Behaviour of Mg-Al Based Insitu Composites for Biomedical Applications

Ayush Saxena  
Mechanical Engineering Department, IFTM University

Vaibhav Trivedi  
Mechanical Engineering Department, IFTM University

Ankur Goel  
Sri sai super speciality Hospital

<https://doi.org/10.5109/7430651>

---

出版情報 : Evergreen. 13 (2), pp.750-755, 2026-06. 九州大学グリーンテクノロジー研究教育センター  
バージョン :  
権利関係 : Creative Commons Attribution 4.0 International



# Synthesis, Characterization and Mechanical Behaviour of Mg-Al Based Insitu Composites for Biomedical Applications

Ayush Saxena<sup>1,\*</sup>, Vaibhav Trivedi<sup>1</sup>, Ankur Goel<sup>2</sup>

<sup>1</sup>Mechanical Engineering Department, IFTM University, Moradabad 244001, India

<sup>2</sup>Sri sai super speciality Hospital, Moradabad 244001, India

\*Author to whom correspondence should be addressed:

Email: ayushsaxena.me@gmail.com

(Received December 22, 2024; Revised November 29, 2025; Accepted March 12, 2026)

**Abstract:** Magnesium based composites have emerged as potential material in biomedical applications owing to its biocompatibility and strength. Present work fabricates the Magnesium-Aluminium with insitu reinforced zirconium diboride composites (Mg-Al/ZrB<sub>2</sub>). Synthesis was conducted in the presence of Argon gas through electric resistance furnace using stir casting route. XRD analysis was performed to see the presence of elements which confirmed the presence of Mg, Al and ZrB<sub>2</sub> peaks. Further Optical microscopy study was conducted to analysis the behaviour of microstructural features of alloy and composites. It was observed that inclusions of insitu formed ZrB<sub>2</sub> results in significant reduction in average grain size. Further, SEM was employed to see the presence of particle, particles distribution, their shape and size. SEM reveals uniform distribution of ZrB<sub>2</sub> particles with hexagonal morphology. However, some agglomeration is also evident which is due to nano particles size of reinforced particles. Also, some porosity is also visible in composite which is further confirmed through density and porosity investigation. Further the Vickers hardness test and ultimate tensile test was performed to analysis the mechanical behaviour of alloy and composites. Results clearly demonstrate increase in Vickers hardness value by ~ 67% and tensile strength ~ 30 % of composite when compared with Mg-Al alloy.

**Keywords:** Characterization; Fabrication; Insitu composite; mechanical properties; Mg-Al alloy

## 1. Introduction

Magnesium (Mg) and its alloys have garnered significant interest in the recent past owing to their excellent properties for a variety of applications, particularly in the biomedical field. Magnesium's low density (1.74 g/cm<sup>3</sup>), high specific strength, and natural biodegradability make it an attractive material for applications such as orthopedic implants<sup>1</sup>. More importantly, Mg's biocompatibility and ability to degrade in biological environments eliminate the requirement for a second surgery to remove the implant, reducing patient risk and medical costs<sup>2</sup>. However, pure Magnesium suffers from several drawbacks, including low mechanical strength and rapid corrosion rates, which restricts its use in load-bearing applications, magnesium alloys have been developed, with the incorporation of alloying elements such as aluminium (Al) to enhance mechanical strength, corrosion resistance, and overall performance<sup>3</sup>. Mg-Al alloys, such as AZ series alloys (e.g., AZ31, AZ91), are among the most widely researched magnesium alloys. Aluminium serves to increase the hardness and tensile strength of magnesium alloys while

reducing grain size through precipitation hardening. Despite these improvements, Mg-Al alloys still exhibit insufficient mechanical strength and corrosion resistance for long-term biomedical applications, particularly in harsh physiological environments<sup>4</sup>.

As a result, there has been a growing focus on developing Mg-Al-based composites that incorporate ceramic reinforcements to further enhance their mechanical properties and corrosion behavior<sup>5</sup>. Composites offer the advantage of combining the desirable properties of a metal matrix with the high hardness and strength of ceramic reinforcements<sup>6,7</sup>. Among various ceramic reinforcements, zirconium diboride (ZrB<sub>2</sub>) has emerged as a promising candidate due to its excellent hardness, high melting point, and chemical stability<sup>8,9</sup>. ZrB<sub>2</sub>'s high biocompatibility also aligns with the stringent requirements for biomedical applications, making it an ideal reinforcement for Mg-Al-based composites<sup>10</sup>.

The synthesis of Mg-Al based composites has become essential for improving the mechanical characteristics and corrosion resistance of magnesium alloys for biomedical applications<sup>11</sup>. The use of ZrB<sub>2</sub> as an in-situ reinforcement

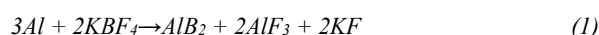
creates a strong interfacial bonding between the matrix and the reinforcement particles, which increases the load transfer and results in better performance under tensile loading<sup>10</sup>. Studies have demonstrated that in-situ formed reinforcements have superior bonding and mechanical properties compared to ex-situ reinforcements, where ceramic particles are mechanically mixed with the metal matrix<sup>12,13</sup>.

Among the various fabrication methods, the stir casting route has been chosen for the synthesis of Mg-Al/ZrB<sub>2</sub> composites due to its simplicity, cost-effectiveness, and ability to produce uniform dispersions of reinforcement particles<sup>14,15</sup>. Stir casting involves an introduction of a reactive element or compound into the molten magnesium alloy to form the reinforcement in-situ, avoiding the issues of poor interfacial bonding and agglomeration that often occur with ex-situ techniques<sup>16</sup>. Furthermore, the use of an argon gas atmosphere during the casting process helps to minimize oxidation, ensuring the quality and purity of the final composite material. Stir casting is a scalable technique, making it suitable for industrial production, which is critical for developing biomaterials for commercial biomedical applications<sup>17,18</sup>. In this context, the current research aims to synthesize in-situ composites using stir casting and to characterize the microstructure and mechanical behavior of the composites. The study focuses on investigating the influence of in-situ formed ZrB<sub>2</sub> particles on the grain structure, hardness, and tensile strength of Mg-Al alloys, with the goal of developing a composite material that meets the mechanical and biocompatibility requirements for biomedical implants. By enhancing the mechanical properties of Mg-Al alloys, the study seeks to overcome the limitation of conventional magnesium alloys and contribute to the development of next-generation biodegradable implants for enhanced load-bearing applications.

## 2. Materials and Methodology

To fabricate the alloy and composites, commercially available pure Mg (purity  $\geq 99.89\%$ ), Al (purity  $\geq 99.9\%$ ), and inorganic salts of Potassium Fluorozirconate (K<sub>2</sub>ZrF<sub>6</sub>) and Potassium tetrafluoroborate (KBF<sub>4</sub>) were procured from India mart. To fabricate the alloy, Mg and Al were taken in the ratio of 95 and 5 weight percent respectively. Initially, the furnace temperature was set at 680°C, and the required amount of Mg and Al in the form of small ingots were kept in graphite crucible having capacity of 5 liter. The heating rate was set 4°C/minute, and holding time was set for 45 minutes. The continuous supply of Argon gas was maintained to create inert atmosphere. After holding for 45 minutes at 680°C the molten alloy was poured into preheated (at 200°C for 2 hour) cast iron Mold having size of 50mm × 50 mm × 170 mm. For the fabrication of composites, initially the furnace temperature was set at 780°C, and required amount of Al

ingots was kept in graphite crucible was placed in furnace. Once the temperature reached at 780°C, the preheated (at 120°C for 1 hour to remove the moisture presents) inorganic salts of K<sub>2</sub>ZrF<sub>6</sub> and KBF<sub>4</sub> wrapped in Al foil was charged into furnace. To form insitu ZrB<sub>2</sub>, intermittent stirring (10 minutes stirring followed by 3 minutes holding) using mechanical stirrer having stainless steel blade was performed for 39 minutes at 200 rotations per minute (rpm). Once the reaction was completed the temperature was lowered at 680°C, and small ingots of preheated (at 100°C for 1 hour) Mg was incorporated into melts and was hold till the Mg was in molten condition. After the melting of Mg, once again the 10 minutes stirring was performed at 200 rpm for homogenization. Finally, the casted samples were poured in preheated mould and allowed to cool at atmospheric temperature. The three composites were fabricated having ZrB<sub>2</sub> weight percentage (wt. %) 1, 3, and 5 respectively. During the whole fabrication process of composites, the continuous supply of Ar gas was maintained. The following likely reaction may have taken place to form the insitu ZrB<sub>2</sub> particles in the melts. In the reactions, Aluminum reacts with the boron obtained from the decomposition of KBF<sub>4</sub> to form AlB<sub>2</sub> which is an intermediate boride. In the presence of Al, K<sub>2</sub>ZrF<sub>6</sub> decomposes and forms Al<sub>3</sub>Zr. Now both AlB<sub>2</sub> and Al<sub>3</sub>Zr are intermediate forms that combines together to form ZrB<sub>2</sub> (an in situ formation) within the Al matrix and releasing excess Al back to the melt. The reaction takes place on the basis of negative Gibbs free energy concept. The decomposition of KBF<sub>4</sub> and K<sub>2</sub>ZrF<sub>6</sub> is occurred due to the presence of Al, which is a strong reducing agent. At last, thermodynamically stable compounds are formed in which total enthalpy decreases and net entropy increases<sup>19</sup>.



## 3. Characterization and Testing

Desktop XRD of Malvern Pananalytical technique was employed to find the peaks present in the alloy and composites. XRD study was performed for 2θ values of 10°-90° with scan rate of 10° per minute. Because, at an angle of less than 10°, it has been observed from the literature that the peaks obtained are weak and has a probability of overlapping with noise or amorphous phase. Whereas, at an angle greater than 90°, the noise increases that leads to significant drop in the intensity. Optilux optical microscopy of Lietz was used to analyze the optical microstructure of alloy and composites. The square cross section of sample (20 mm × 20 mm × 10 mm) was prepared from as cast sample. Set of emery papers was used for grinding the surface followed by cloth polishing of



**Fig.1:** (a) stir casting setup (b) Mold of cast iron (c) as cast sample (d) prepared sample for optical microscopy and Vickers hardness study (e) Tensile sample

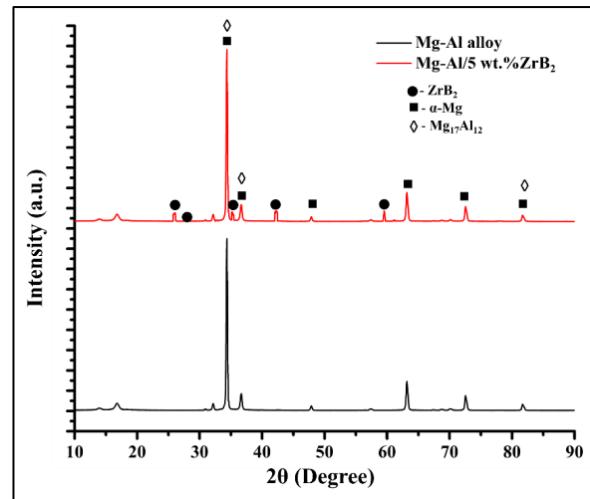
specimen. Once the sample was free from scratch, the acetic Picralwas used as etchant to find out the grain boundaries. Further, JEOL Bench top scanning electron microscopy (SEM) was utilized to see the particles size, shape and distribution of particles in the matrix. Experimental density was determined using Archimedes principal and porosity was calculated using ratio of difference of theoretical density to experimental density over theoretical density.

To study the impact of reinforced particles on mechanical properties, the hardness and tensile test was performed using Vickers hardness and ultimate tensile strength set up according to ASTM standard E384 and E8 respectively. Figure 1 shows the stir casting set up; Mold made of cast iron along with prepared samples for various study.

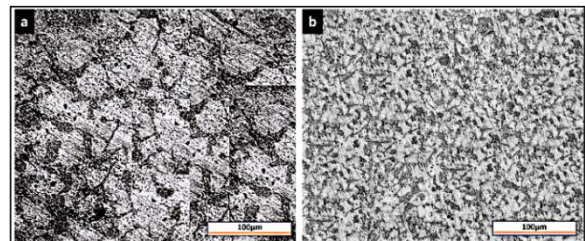
#### 4. Results and Discussion

Figure 2 presents the X ray diffractometer (XRD) image of Mg-Al alloy and Mg-Al/5wt.% ZrB<sub>2</sub> composites. It can see from the image that in the case of alloy, the peaks of Mg and alloy of Mg i.e. Mg<sub>17</sub>Al<sub>12</sub> is present while for composites along with peaks of Mg and MG<sub>17</sub>Al<sub>12</sub>, presence of ZrB<sub>2</sub> can be seen, which confirms the presence of reinforced particles in matrix.

Figure 3 shows the optical microstructure (OM) of Mg-Al alloy and Mg-Al/5 wt.% ZrB<sub>2</sub> composite. Figure 3 (a) shows the OM of Mg-Al alloy. The white region shows the  $\alpha$ - Mg (magnesium-rich phase), while the darker region presents the Mg<sub>17</sub>Al<sub>12</sub> phase. Figure 3 (b) shows the OM of Mg-Al/5 wt.% ZrB<sub>2</sub>. A finer grain structure can be seen in the case of composites. This reduction in grain size is due to the insertion of reinforced particles, which act as a secondary phase leading to the region of generation of



**Fig.2:** XRD of Mg-Al alloy and Mg-Al/5wt.% ZrB<sub>2</sub> composite



**Fig.3:** Optical microstructure of (a) Mg-Al alloy (b) Mg-Al/5 wt.% ZrB<sub>2</sub> composite

nucleation sites, which further hinders grain growth. Further, mismatch in the thermal coefficient of hard ZrB<sub>2</sub> particles with Mg-Al causes a restriction in grain growth, thus finer grain structure<sup>19-21</sup>. The average grain size was determined in accordance with ASTM E112 standard. At least five random fields were analyzed per sample to ensure statistical accuracy and given in Figure 5<sup>22</sup>). In the linear intercept method, a set of straight, evenly spaced lines is superimposed over a micro structural image. These lines intersect grain boundaries, and each intersection point is counted. The basic idea is that the more the intersections the smaller the grain size. The average grain size is then calculated by dividing the total length of all test lines by the number of intercepts. This gives an estimate of the mean linear intercept length, which represents the average grain diameter. This can be observed that for Mg-Al alloy the average grain size is in the range of 27 $\mu$ m while decreases with addition of ZrB<sub>2</sub> and is observed to be lowest with reinforcement of 5 wt.% of ZrB<sub>2</sub> having order of 8 $\mu$ m.

Figure 4 presents the SEM image of Mg-Al/5wt.% ZrB<sub>2</sub> composites. This can be observed from the Figure 4(a) that particles are uniformly distributed with slight agglomerations which may be because of very fine size of the particles. Further Figure 4(b) shows the SEM image of particles at higher magnification which clearly demonstrate the shape and size of reinforced particles i.e. hexagonal shape<sup>23-25</sup>). Also, the average particles size was

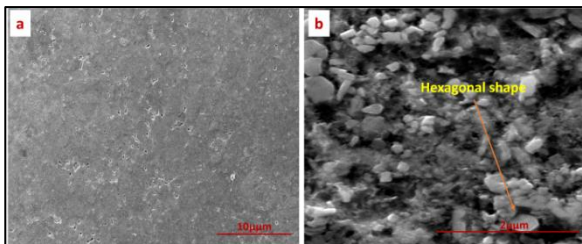


**Fig.4:** Scanning electron microscopy of (a) Mg-Al alloy (b) Mg-Al/5 wt.% ZrB<sub>2</sub> composite.

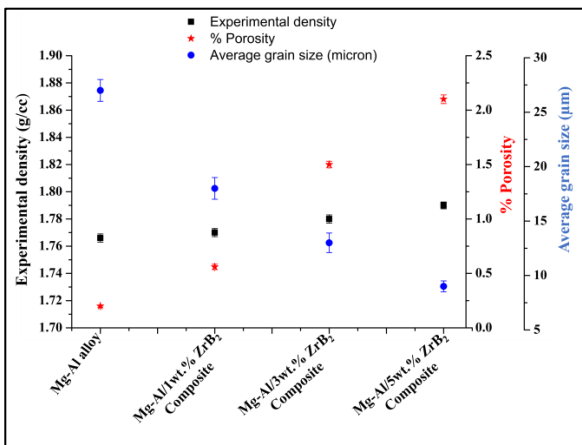


**Fig.5:** Density (g/cm<sup>3</sup>), % Porosity, and average grain size (μm) of alloy and composites

determined using Image J software from SEM micrograph and found to be 0.1 μm.

Figure 5 shows the physical properties (i.e. experimental densities and % porosity) and average grain size of the alloy and composites (Figure 4). It can be observed from Figure 4. That the mixing of ZrB<sub>2</sub> and Al is fairly homogenous however, at some sites the ZrB<sub>2</sub> agglomeration is noted which is probably attributed to the uneven cooling and shrinkage of boundaries due to solidification. The observed decrease in experimental density, despite the use of high-density reinforcement particles can be attributed to the presence of micro-porosity and possible particle agglomeration during solidification<sup>26</sup>. These defects reduce the overall compactness of the matrix, leading to a lower measured density compared to the theoretical value<sup>27</sup>. This observed porosity may be attributed to more stirring speed and trapping of atmospheric gases at the time of pouring<sup>28</sup>. In addition to, phenomena such as grain boundary pinning (due to local grain coarsening), etching, and settlement of ZrB<sub>2</sub> particle due to not rapidly cooling are some of the probable reasons of density difference.

Figure 6 presents the mechanical (hardness and tensile strength) of Mg-Al alloy and its composites. This can be seen that with addition of ZrB<sub>2</sub>, there is significant improvement in hardness with respect to Mg-Al alloy and maximum for Mg-Al/ 5 wt. % ZrB<sub>2</sub> composites. This is due to high hardness properties of reinforced particles which results in an increase in bulk hardness. Further, reinforced

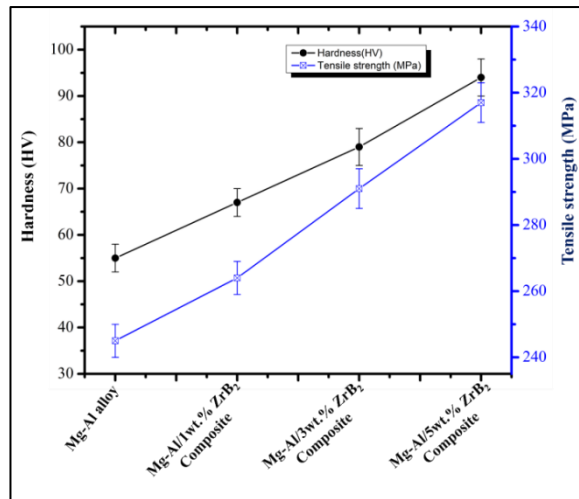


**Fig.6:** Hardness (HV), and tensile strength (MPa) of alloy and composites

ZrB<sub>2</sub> particles and Mg-Al alloy exhibits mismatch in thermal coefficient of expansion which results in increase in dislocation density thus causing restriction to plastic deformation further leading to rise in hardness<sup>10,29,30</sup>.

Tensile behaviour of Mg-Al alloy and its composites was investigated at atmospheric temperature as given in Figure 6. This can be observed that with reinforcement of ZrB<sub>2</sub> particles, there is a significant rise in tensile strength of matrix of Mg-Al alloy and is maximum for Mg-Al/5 wt.% ZrB<sub>2</sub>. The increase in tensile strength results from the refinement of matrix grains caused by the introduction of ZrB<sub>2</sub> particles, as explained in the previous section. This grain refinement leads to improved tensile strength, which can be explained by the Hall-Petch relationship in which the particles of ZrB<sub>2</sub> serve as heterogeneous nucleation sites that result in refined grain structure in the Al metal matrix. During tensile loading, dislocations are generated, and the second-phase particles obstruct their movement due to decrease in grain size and increase in total grain boundaries area, thereby contributing to the strengthening effect<sup>31-34</sup>. Additionally, the mismatch in the thermal expansion coefficients between the matrix and particles further raises the dislocation density, enhancing the strength<sup>35</sup>.

### 5. Conclusions

The Mg-Al alloy and Mg-Al/ZrB<sub>2</sub> in situ composites were successfully synthesized using the stir casting technique, with ZrB<sub>2</sub> reinforcement varying from 0 to 5 wt.%. Key observations include:

The in-situ formation of ZrB<sub>2</sub> particles significantly refined the grain structure, achieving up to ~70% grain refinement with 5 wt.% ZrB<sub>2</sub> addition.

Homogeneous dispersion of ZrB<sub>2</sub> particles in the matrix was achieved, contributing to enhanced mechanical properties.

Vickers hardness increased notably from 55 HV to 92 HV at 5 wt.% ZrB<sub>2</sub>.

Tensile strength improved by ~30% for the Mg-Al/5 wt.% ZrB<sub>2</sub> composite compared to the base Mg-Al alloy.

With superior hardness and tensile strength, the newly developed Mg-Al/5 wt.% ZrB<sub>2</sub> composite holds promising potential for biomedical applications, particularly in load-bearing implants and devices where strength and biocompatibility are crucial.

## References

- 1) S. V. S. Prasad, S. B. Prasad, K. Verma, R. K. Mishra, V. Kumar, and S. Singh, "The role and significance of Magnesium in modern day research-A review," *J. Magnesium Alloys*, 10(1), 1–61 (2022). <https://doi.org/10.1016/j.jma.2021.05.012>.
- 2) V. Tsakiris, C. Tardei, and F. M. Clicinschi, "Biodegradable Mg alloys for orthopedic implants – A review," *J. Magnesium Alloys*, 9(6), 1884–1905 (2021). <https://doi.org/10.1016/j.jma.2021.06.024>.
- 3) K. Munir, J. Lin, C. Wen, P. F. A. Wright, and Y. Li, "Mechanical, corrosion, and biocompatibility properties of Mg-Zr-Sr-Sc alloys for biodegradable implant applications," *Acta Biomater.*, 102, 493–507 (2020). <https://doi.org/10.1016/j.actbio.2019.12.001>.
- 4) Z. Yang, J. Li, J. Zhang, G. Lorimer, and J. Robson, "Review on research and development of magnesium alloys," *Acta Metall. Sin. (Engl. Lett.)*, 21, 313–328 (2008). [https://doi.org/10.1016/S1006-7191\(08\)60054-X](https://doi.org/10.1016/S1006-7191(08)60054-X).
- 5) J. Y. Ren, G. C. Ji, H. R. Guo, Y. M. Zhou, X. Tan, W. F. Zheng, Q. Xing, J. Y. Zhang, J. R. Sun, H. Y. Yang, F. Qiu\* and Q. C. Jiang, "Nano-enhanced phase reinforced magnesium matrix composites: A review of the Matrix, Reinforcement, Interface Design, Properties and Potential Applications," *Materials*, 17(10), 2454 (2024). <https://doi.org/10.3390/ma17102454>.
- 6) R. Maurya, V. Kumar, S. Gautam, S. Bharti, and S. Mallika, "Investigation of microstructural and mechanical characteristics of Al-ZrO<sub>2</sub> composites fabricated by stir casting," *Interactions*, 245, 301 (2024). <https://doi.org/10.1007/s10751-024-02163-x>.
- 7) L. Ranakoti, P. Bhandari, M. K. Gupta, K. Kumar, S. Bhatia, S. Kosaraju, and Jarnail Singh, "Ceramic matrix composite reinforced with glass and walnut shell filler: Influence of mesh size on its mechanical properties," *Mater. Today Proc.*, (2023). <https://doi.org/10.1016/j.matpr.2023.08.106>.
- 8) V. Kumar, A. Singh, Ankit, and Gaurav Gautam, "A comprehensive review of processing techniques, reinforcement effects, and performance characteristics in copper-based metal matrix composites," *Interactions*, 245, 357 (2024). <https://doi.org/10.1007/s10751-024-02200-9>.
- 9) A. L. Chamberlain, W. G. Fahrenholtz, G. E. Hilmas, and D. T. Ellerby, "High-strength zirconium diboride-based ceramics," *J. Am. Ceram. Soc.*, 87, 1170–1172 (2004).
- 10) V. Kumar, A. Mishra, S. Mohan, and A. Mohan, "Fabrication of stir cast ZA/ZrB<sub>2</sub> reinforced in-situ composites," *Mater. Res. Express*, 6(12) (2019). <https://doi.org/10.1088/2053-1591/ab53f2>.
- 11) A. Verma and S. Ogata, "Magnesium based alloys for reinforcing biopolymer composites and coatings: A critical overview on biomedical materials," *Adv. Ind. Eng. Polym. Res.*, 6(4), 341–355 (2023). <https://doi.org/10.1016/j.aiepr.2023.01.002>.
- 12) J. D. R. Selvam and I. Dinaharan, "In situ formation of ZrB<sub>2</sub> particulates and their influence on microstructure and tensile behavior of AA7075 aluminum matrix composites," *Eng. Sci. Technol. Int. J.*, 20(1), 187–196 (2017). <https://doi.org/10.1016/j.jestch.2016.09.006>.
- 13) S. Tripathi, A. Bhadauria, A. Tiwari, and A. K. Tiwari, "Effect of carbonaceous reinforcements on mechanical properties of ZrB<sub>2</sub>-SiC composites via nanoindentation study," *Diamond Relat. Mater.*, 140, 110537 (2023). <https://doi.org/10.1016/j.diamond.2023.110537>.
- 14) V. Kumar, L. Ranakoti, G. Gautam, A. Negi, T. Singh, "Erosive wear and topographical study of zinc-aluminum based composite reinforced with in-situ formed ZrB<sub>2</sub> particles," *Results Eng.*, 22, 102346 (2024). <https://doi.org/10.1016/j.rineng.2024.102346>.
- 15) E. Suneesh, and M. Sivapragash, "Comprehensive studies on processing and characterization of hybrid magnesium composites," *Mater. Manuf. Process*, 33(12), 1324–1345(2018). <https://doi.org/10.1080/10426914.2018.1453155>.
- 16) M. A. M. D. L. Sanchez, J. Duarte, B. J. Santos, L.E. C. Garcia, J. M. Ruiz-Roman, and F. J. Elorza, "Stir Casting Routes for Processing Metal Matrix Syntactic Foams: A Scoping Review," *Processes*, 10(3), 478 (2022). <https://doi.org/10.3390/pr10030478>.
- 17) P. K. Gurmaita, R. Ponggen, and S. K. Gurmaita, "A7075 alloy reinforced metal matrix composites fabricated through stircasting route: a review," *Int. J. Cast Met. Res.*, 37(3), 208–255(2024). <https://doi.org/10.1080/13640461.2024.2355634>.
- 18) J. Grilo, V. H. Carneiro, J. C. Teixeira, H. Puga, "Manufacturing methodology on casting-based aluminium matrix composites: systematic review," *Metals*, 11(3), 436(2021). <https://doi.org/10.3390/met11030436>.
- 19) P. Pesode, S. Barve, S. V. Wankhede, and A. Ahmad, "Sustainable materials and technologies for biomedical applications." *Adv. Mater. Sci. Eng.*, 2023(1),

- 6682892(2023). <https://doi.org/10.1155/2023/6682892>
- 20) D. Padalia, U. Kumar, P. Bhandari, J. Dalal, L. Ranakoti, and T. Singh, "Tuning the structural, optical, and dielectric properties of europium-doped barium titanate ceramics," *J. Mater. Sci.: Mater. Electron.*, 35 (2024). <https://doi.org/10.1007/s10854-024-12984-9>.
  - 21) D. Chandra and N. Chauhan, "Effect of Ceramic Coating on Mechanical Properties of AZ31 Magnesium Alloy," *Evergreen*, 11, 1732–1739 (2024). <https://doi.org/10.5109/7236825>.
  - 22) ASTM, "Standard test methods for determining average grain size," *ASTM E112*, 4–20 (1996).
  - 23) V. Kumar, G. Gautam, A. Singh, V Singh, S Mohan, and A. Mohan, "Tribological behaviour of ZA/ZrB2 in situ composites using response surface methodology and artificial neural network," *Surf. Topogr.: Metrol. Prop.*, 10(4), 045001 (2022). <https://doi.org/10.1088/2051-672X/ac9426>.
  - 24) K. Kirman, H. A. Suhartono, O. Ivano, and Y. Irawadi, "Enhancing aluminum alloys with nanoparticle reinforcement," *Evergreen*, 11, 2720–2727 (2024). <https://doi.org/10.5109/7236911>.
  - 25) H. Cao, C. Wang, Q. Shan, J. Che, Z. Luo, L. Wang, and M. Huang, "Kinetic analysis of pore formation in die-cast metals and influence of absolute pressure on porosity," *Vacuum*, 168, 108828 (2019). <https://doi.org/10.1016/j.vacuum.2019.108828>.
  - 26) H. Kumar, V. Kumar, D. Kumar, S. Singh, "Wear Behavior of Friction Stir Processed Copper-Cerium Oxide Surface Composites," *Evergreen*, 10, 78–84 (2023). <https://doi.org/10.5109/6781043>.
  - 27) V. Kumar, G. Gautam, Ankit, A. Mohan, and S. Mohan, "Correlating surface topography of relaxed layer of ZA/ZrB2 in situ composites to wear and friction," *Surf. Topogr.: Metrol. Prop.*, 11(2) (2023). <https://doi.org/10.1088/2051-672X/acc881>.
  - 28) L. Ranakoti, A. Negi, B. Gangil, P. Bhandari, R. Singh, S. Sharma, S. Dwivedi, P. Bains, E. Makki, & M. Abbas, "Physicomechanical, microstructural morphological, and thermal characterizations of jute and coconut husk-based natural fibers reinforced hempcrete hurd composites for building and construction applications," *Biomass Convers. Biorefin.*, 1–12 (2024). <https://doi.org/10.1007/s13399-024-05682-3>.
  - 29) W. Ma, B. Zhenyu, S. Chufeng, A. Yulong, and Z. Xiaoqin, "Influence of porosity distribution and toughening effect on the tribological properties of Al2O3-Y2O3 coatings with different Y2O3 contents," *Ceram. Int.*, 51(6), 7809-7824 (2024). <https://doi.org/10.1016/j.ceramint.2024.12.218>.
  - 30) Y. J. Ge, R. F. Guo, and P. Shen, "Wettability and interfacial reactions in Al–Mg–Si/SiC and Al–Mg–Si/SiO2 systems," *Mater. Charact.*, 219, 114599 (2024). <https://doi.org/10.1016/j.matchar.2024.114599>.
  - 31) R. Lumley, A. Morton, I. Polmear, "Nanoengineering of metallic materials," Woodhead Publishing, 219–250 (2006). <https://doi.org/10.1533/9781845691189.219>.
  - 32) V. Kumar, G. Gautam, A. Mohan and S. Mohan, "Tribology of Insitu Zn-Al/ZrB2 Composites in Reciprocating Motion," *Int. Metalcast*, 17, 182–194 (2023). <https://doi.org/10.1007/s40962-022-00764-2>.
  - 33) A. Kumar, R. Rana, R. Purohit, M. Baghel, A. Namdev, and R. Kumar, "Investigation of Tensile behaviour, Seizure Conditions and Frictional Characteristics of Al-Zn-Cu-Mg Alloy based Composites," *Silicon*, 15(18), 7903-7915 (2023). <https://doi.org/10.1007/s12633-023-02627-9>.
  - 34) C. L. Li, Q. S. Mei, J. Y. Li, F. Chen, Y. Ma, and X. M. Mei, "Hall-Petch relations and strengthening of Al-ZnO composites in view of grain size relative to interparticle spacing," *Scr. Mater.*, 153, 27–30 (2018). <https://doi.org/10.1016/j.scriptamat.2018.04.042>.
  - 35) O. Matvienko, O. Daneyko, T. Kovalevskaya, A. Khrustalyov, I. Zhukov, and A. Vorozhtsov, "Investigation of Stresses Induced Due to the Mismatch of the Coefficients of Thermal Expansion of the Matrix and the Strengthening Particle in Aluminum-Based Composites," *Metals*, 11(2), 279 (2021). <https://doi.org/10.3390/met11020279>.